JBC RESEARCH ARTICLE

Nitration-mediated activation of the small GTPase RhoA stimulates cellular glycolysis through enhanced mitochondrial fission

Received for publication, September 2, 2022, and in revised form, February 14, 2023 Published, Papers in Press, February 24, 2023,
https://doi.org/10.1016/j.jbc.2023.103067

Qing Lu[1,2], Xutong Sun[1,2], Manivannan Yegambaram[3], Wojciech Ornatowski[3], Xiaomin Wu[3], Hui Wang[3], Alejandro Garcia-Flores[1,2], Victoria Da Silva[1,2], Evgeny A. Zemskov[1,4], Haiyang Tang[1,2], Jeffrey R. Fineman[5,6], Kim Tieu[2], Ting Wang[1,2], and Stephen M. Black[1,2,4,*]

From the [1]Center of Translational Science, Florida International University, Port St Lucie, Florida, USA; [2]Department of Environmental Health Sciences, Robert Stempel College of Public Health and Social Work, Florida International University, Miami, Florida, USA; [3]Department of Medicine, University of Arizona Health Sciences, Tucson, Arizona, USA; [4]Department of Cellular Biology & Pharmacology, Howard Wertheim College of Medicine, Florida International University, Miami, Florida, USA; [5]Department of Pediatrics and [6]Cardiovascular Research Institute, University of California San Francisco, San Francisco, California, USA

Reviewed by members of the JBC Editorial Board. Edited by Qi-Qun Tang

Mitochondrial fission and a Warburg phenotype of increased cellular glycolysis are involved in the pathogenesis of pulmonary hypertension (PH). The purpose of this study was to determine whether increases in mitochondrial fission are involved in a glycolytic switch in pulmonary arterial endothelial cells (PAECs). Mitochondrial fission is increased in PAEC isolated from a sheep model of PH induced by pulmonary overcirculation (Shunt PAEC). In Shunt PAEC we identified increases in the S^{616} phosphorylation responsible for dynamin-related protein 1 (Drp1) activation, the mitochondrial redistribution of Drp1, and increased cellular glycolysis. Reducing mitochondrial fission attenuated cellular glycolysis in Shunt PAEC. In addition, we observed nitration-mediated activation of the small GTPase RhoA in Shunt PAEC, and utilizing a nitration-shielding peptide, NipR1 attenuated RhoA nitration and reversed the Warburg phenotype. Thus, our data identify a novel link between RhoA, mitochondrial fission, and cellular glycolysis and suggest that targeting RhoA nitration could have therapeutic benefits for treating PH.

Congenital heart defects with increased pulmonary blood flow (PBF) are associated with the development of increased pulmonary vascular reactivity and pulmonary hypertension (PH) (1–3). In the postnatal period, the presence of large communications at the level of the ventricles (*e.g.*, ventricular septal defect) or great vessels (*e.g.*, truncus arteriosus) exposes the pulmonary circulation to abnormal elevations in blood flow and pressure, which results in progressive structural and functional abnormalities of the pulmonary vasculature (2, 4–12). While there have been advances in the understanding of some aspects of the pathobiology of many etiologies of pulmonary vascular disease (PVD), such as defining the importance of alterations in NO-signaling (13–19), a deep understanding of the inducing and regulatory pathways involved in PVD remain poorly understood. Furthermore, current therapies are limited to augmenting the NO-cGMP or prostacyclin cascades or blocking the ET-1 cascade. Thus, disease severity is targeted and not disease pathobiology. Metabolic reprogramming is a critical component of PH (20, 21). We, and others, have shown that, like cancer, the development of PVD relies on metabolic reprogramming to favor glycolysis (22–43). Furthermore, we have identified a causal link between this metabolic reprogramming and the development of the hyperproliferative endothelial phenotype in our lamb model of increased PBF (24). This link is, in part, because proliferating cells have different metabolic needs than nonproliferating ones (44); in addition to generating ATP, proliferating cells must also produce biosynthetic precursors such as nucleic acids and lipids required for cell division (45, 46). Utilizing our ovine model of a congenital heart defect with increased PBF and pressure (Shunt), we have linked the disruption of mitochondrial function and the stimulation of aerobic glycolysis, *i.e.*, the Warburg effect, to the development of endothelial dysfunction (24, 47–50) and increased remodeling (51, 52) in this setting. The mechanisms by which pathologic mechanical forces produce metabolic reprogramming need to be better understood.

Mitochondria are highly dynamic organelles, forming elongated tubes through fusion and, through fission, splitting into small, less connected mitochondria (53). Fusion permits mixing the contents between mitochondria and may protect the mitochondria (54). The mitochondrial guanosine triphosphatases mitofusin (Mfn)-1 and -2 and the optic atrophy 1 protein (OPA-1) regulate mitochondrial fusion. Fission occurs through the GTPase activity of dynamin-related protein 1 (Drp1). Drp1 is present in the cytosol and translocates to the mitochondria when activated. Drp1 assembles into oligomeric structures that mechanically constrict and fragment the

* For correspondence: Stephen M. Black, stblack@fiu.edu.

mitochondria (55). The seminal work of Archer's group has shown that increased mitochondrial fission in the smooth muscle cells correlates with the development of advanced forms of PH through the activation of Drp1 (56, 57). Although both a Warburg phenotype and an increase in mitochondrial fission are associated with PH development, it is unclear whether there is a mechanistic link between the two processes. Thus, in this study, we focused on determining a causal link between increases in mitochondrial fission and increases in glycolysis using pulmonary arterial endothelial cells isolated from our Shunt lamb model of PH (Shunt PAEC). Our data demonstrate that mitochondrial fission is increased in Shunt PAEC, which correlates with increased Drp1 activity and a Warburg phenotype. Increasing mitochondrial fusion by inhibiting Drp1 or the adenoviral-mediated overexpression of MFN2 could decrease cellular glycolysis in Shunt PAEC. Furthermore, we identified increased RhoA-ROCK signaling, mediated *via* nitrated RhoA, as being responsible for the activation of Drp1 *via* increases in pS^{616} and showed that decreasing RhoA nitration using the shielding peptide NipR1 (58) decreased mitochondrial fission, reduced cellular glycolysis, and restored mitochondrial function.

Results

Increased mitochondrial fission is associated with increased cellular glycolysis in PAEC isolated from shunt lambs

We evaluated three pairs of PAECs isolated from Control and Shunt lambs using fluorescent microscopy to examine changes in mitochondrial morphology (Fig. 1*A*). The mitochondrial aspect ratio (Fig. 1*B*) and the number of branches (Fig. 1*C*) and junctions (Fig. 1*D*) are all lower in PAEC isolated from Shunt compared with Control lambs, indicating more mitochondrial fission. Western blot analysis further confirmed

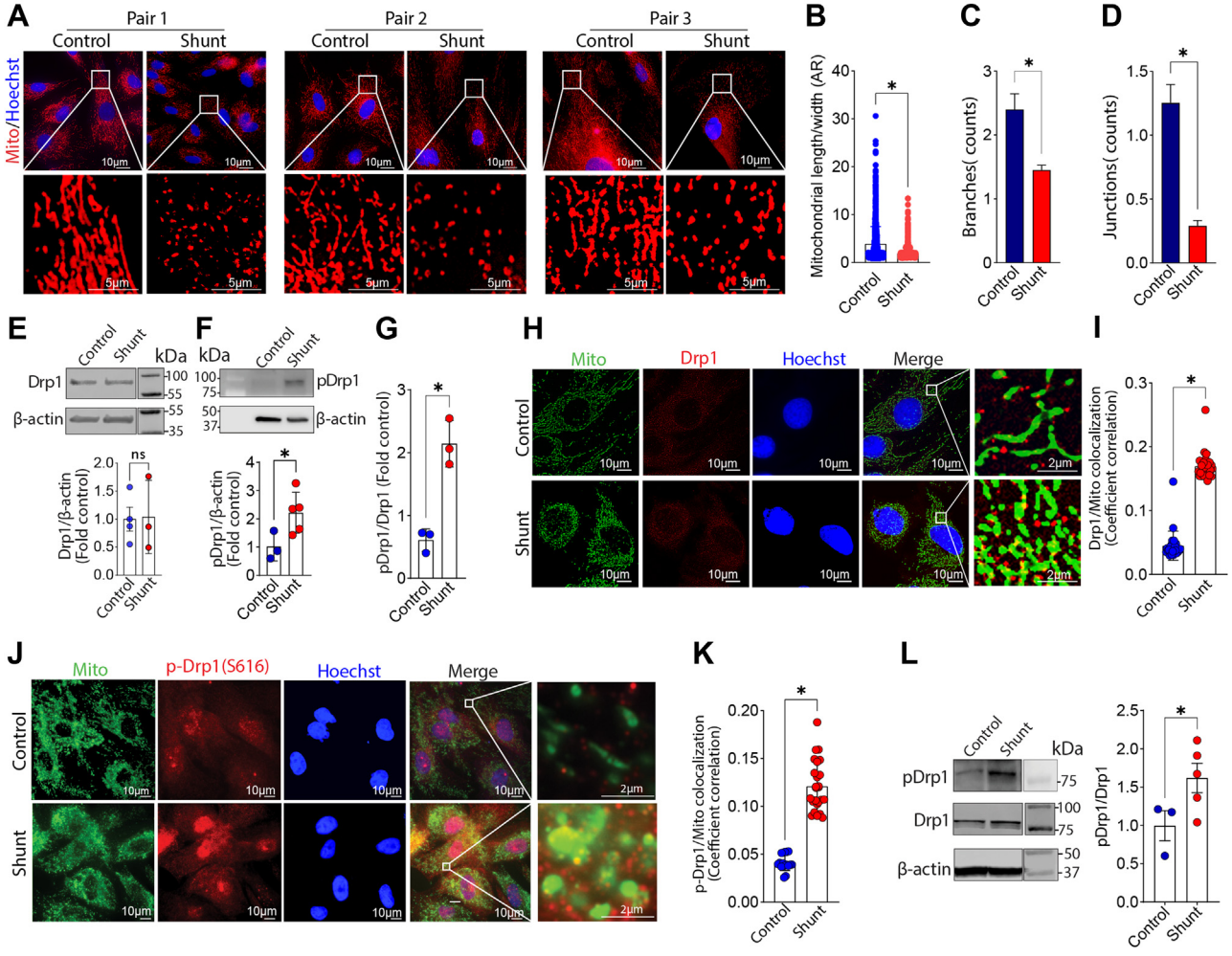

Figure 1. Pulmonary arterial endothelial cells (PAECs) isolated from lambs with pulmonary hypertension exhibit increased mitochondrial fission. PAECs isolated from three pairs of Control and Shunt lambs and mitochondria labeled with MitoTracker (*A*) were analyzed to examine changes in mitochondrial network dynamics. Our data indicate that there are significant decreases in the mitochondrial aspect ratio (AR, *B*), the number of branches (*C*), and junctions (*D*) in PAEC isolated from Shunt lambs, indicative of increased mitochondrial fission. Western blot analysis shows that, although total Drp1 (*E*) levels are unchanged in Shunt PAEC, pS^{616}Drp1 (*F*) and the pS^{616}Drp1:total Drp1 ratio (*G*) are increased. Representative images are shown. β-Actin was used to normalize protein loading. Immunofluorescence microscopy shows increases in the localization of the mitochondrial fission protein Drp1 (*H* and *I*), and its activated phosphorylated form, pS^{616}Drp1, in the mitochondria of Shunt PAEC (*J* and *K*). Western blot analysis shows that the ratio of pS^{616}Drp1 to total Drp1 increases in peripheral lung tissue prepared from 4-week-old Shunt, compared with Control lambs (*L*). Representative images are shown. β-Actin was used to normalize protein loading. The scale bar represents 10 μm. Data are mean ± SE. $*p < 0.05$ *versus* Control PAEC or Control lung.

that, although the total Drp1 protein expression level was not altered (Fig. 1*E*), the activating phosphorylation of Drp1 at S616 was significantly higher in Shunt PAEC (Fig. 1*F*) increasing the pS16Drp1:Drp1 ratio (Fig. 1*G*). Further immunofluorescence analysis identified increased colocalization of total Drp1 (Fig. 1, *H* and *I*) and pS616Drp1 (Fig. 1, *J* and *K*) with the mitochondria in Shunt PAEC. We also observed an increase in the pS616Drp1: total Drp1 ratio in peripheral lung tissue extracts prepared from Shunt lambs, indicating that the increase in Drp1 activation we observed in cultured PAEC is recapitulated in the whole lung (Fig. 1*L*). Differences in expression between the whole lung and isolated PAECs may be due to increased Drp1 expression in other cell types. The increase in mitochondrial fission in Shunt PAEC was also correlated with decreased mitochondrial membrane potential (Fig. 2*A*) and increased generation of mitochondrial reactive oxygen species (mt-ROS) (Fig. 2*B*). The increase in mt-ROS was associated with increased HIF1α protein levels (Fig. 2*C*) and higher basal glycolysis(Fig. 2*D*). Although the addition of the Drp1 inhibitor, mdivi-1, did not change any of the three measured parameters of mitochondrial fission in PAEC from Control lambs (Fig. 3*A*), it increased the mitochondrial aspect ratio (Fig. 3*B*) and the number of branches (Fig. 3*B*) and junctions (Fig. 3*B*) in Shunt PAEC indicative of a decrease in mitochondrial fission. Mdivi-1 treatment also restored the mitochondrial membrane potential (Fig. 3*C*), reduced mt-ROS levels (Fig. 3*D*), and decreased HIF1α protein levels (Fig. 3*E*) in Shunt PAEC, indicating a restoration of mitochondrial function. The reductions in HIF1α induced by mdivi-1 resulted in a decrease in cellular glycolysis in Shunt PAEC (Fig. 3, *F*–*I*). These data indicate that increased generation of mitochondrial ROS, mitochondrial dysfunction, and cellular glycolysis are closely related to mitochondrial fission.

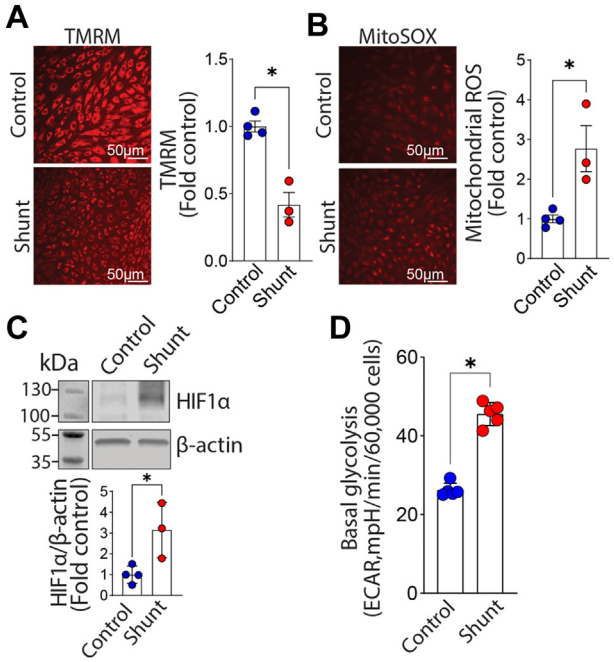

Figure 2. Evidence of mitochondrial dysfunction and increased glycolysis in pulmonary arterial endothelial cells (PAECs) isolated from lambs with pulmonary hypertension. The mitochondrial membrane potential is decreased in Shunt PAEC (*A*) and mt-ROS levels are increased (*B*), indicating mitochondrial dysfunction. Western blot analysis shows that the glycolysis activating transcription factor HIF1α protein levels are increased in Shunt PAEC (*C*). Representative images are shown. β-Actin was used to normalize protein loading. The increase in HIF1α correlates with increased basal glycolysis determined using a Seahorse analyzer and the glycolysis stress test (*D*). Data are mean ± SE. *$p < 0.05$ *versus* Control PAEC.

Increasing mitochondrial fusion reduces cellular glycolysis in PAEC isolated from shunt lambs

To further investigate the mechanism underlying the increased mitochondrial fission in Shunt PAEC, we evaluated changes in the mitochondrial fusion proteins, MFN1 and MFN2. MFN2, but not MFN1, protein levels were significantly reduced in Shunt PAEC (Fig. 4, *A* and *B*). Using an adenoviral expression vector to increase MFN2 expression in Shunt PAEC (Fig. 4*C*) we were able to increase the mitochondrial aspect ratio and the number of branches and junctions in Shunt PAEC (Fig. 4, *D*–*G*), indicative of increased mitochondrial fusion. The increased fusion was associated with a reduced cellular glycolytic capacity (Fig. 4, *H*–*K*) and a reduced glycolytic ATP production rate (Fig. 4*L*). The decrease in glycolysis was associated with increases in mitochondrial membrane potential (Fig. 4*M*), reduced mt-ROS levels (Fig. 4*N*), and decreased HIF1α protein levels (Fig. 4*O*). These results again support the conclusion that the disruption in mitochondrial fusion and fission balance in Shunt PAEC underlies the glycolytic phenotype.

Nitration-mediated activation of RhoA is involved in the increased mitochondrial fission in PAEC isolated from shunt lambs

In Shunt PAEC, NO_x levels are decreased (Fig. 5*A*) while cellular superoxide levels (Fig. 5*B*) are increased. These changes correlated with increased peroxynitrite levels in Shunt PAEC (Fig. 5*C*). We have previously shown that the upstream regulator of ROCK, RhoA, is activated by nitration (58, 59). Activated ROCK can phosphorylate Drp1 at S^{616} and stimulate its activity (60, 61). Thus, we next investigated nitration-mediated activation of RhoA-ROCK signaling as the mechanism underlying the activation of Drp1. Both RhoA nitration (Fig. 5*D*) and RhoA activity (Fig. 5*E*) are increased in Shunt PAEC. RhoA nitration (Fig. 5*F*) and RhoA activity (Fig. 5*G*) are also increased in the lung tissue of Shunt lambs, indicating that changes in RhoA nitration and activity are recapitulated in the whole lung. In Control PAEC, the adenoviral-mediated overexpression of a constitutively active mutant of RhoA (RhoA Q63L, CA-RhoA, Figure 6, *A* and *B*) increased $pDrp1S^{616}$ levels (Fig. 6*C*). It also increased the mitochondrial aspect ratio and the number of branches and junctions, indicative of increased mitochondrial fission (Fig. 6, *D*–*G*). Active RhoA also decreased the mitochondrial membrane potential (Fig. 6*H*), increased mt-ROS levels (Fig. 6*I*), and increased HIF1α protein levels (Fig. 6*J*). These changes correlated with increased cellular glycolysis (Fig. 6, *K*–*N*).

We next investigated whether specifically targeting the nitration of RhoA using our previously described nitration

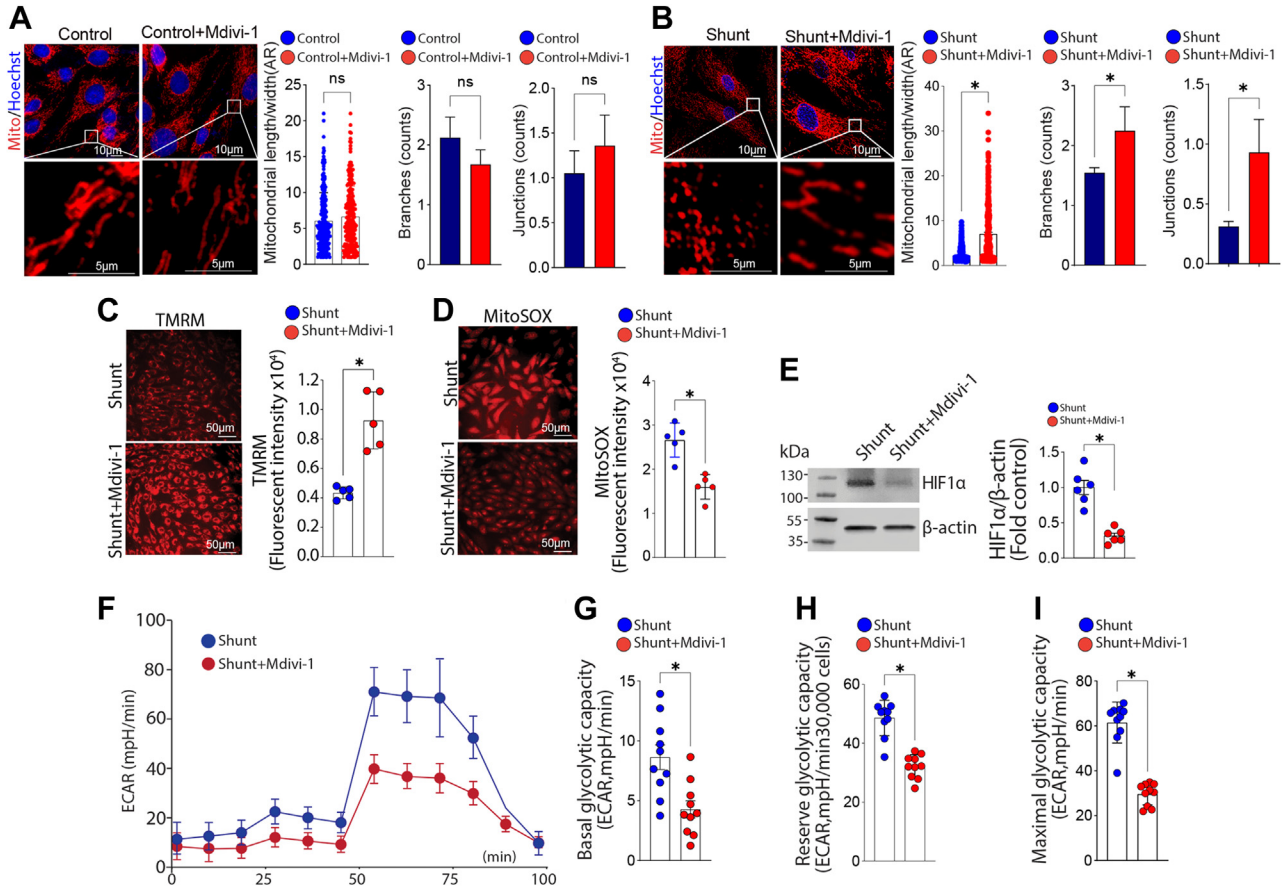

Figure 3. Attenuating mitochondrial fission reduces mitochondrial dysfunction and cellular glycolysis in pulmonary arterial endothelial cells (PAECs) isolated from lambs with pulmonary hypertension. PAECs were treated or not with the Drp1 inhibitor, mdivi-1 (100 μM, 24 h), then the mitochondria were labeled with MitoTracker, and effects on mitochondrial fission were analyzed. Mdivi-1 exposure does not change the aspect ratio (AR), branches, and junctions counts in Control PAEC (*A*), but increases the AR and the number of mitochondrial branches and junctions in Shunt PAEC (*B*), indicative of increased mitochondrial fusion. Mdivi-1 also increases the mitochondrial membrane potential in Shunt PAEC (*C*) and decreases mt-ROS levels (*D*). Western blot analysis shows that HIF1α protein levels are decreased by mdivi-1 in Shunt PAEC (*E*). Representative images are shown. β-Actin was used to normalize protein loading. Mdivi-1 also decreases cellular glycolysis in Shunt PAEC (*F*), as evidenced by decreases in basal (*G*), reserve (*H*), and maximal (*I*) glycolytic capacity. The scale bar represents 10 μm. Data are mean ± SE. $*p < 0.05$ *versus* untreated Shunt PAEC.

shielding peptide, NipR1 (58, 59) could attenuate the increases in mitochondrial fission and cellular glycolysis in Shunt PAEC. Although the addition of the NipR1 did not change any of the three measured parameters of mitochondrial fission in PAEC from Control lambs (Fig. 7*A*), it increased the mitochondrial aspect ratio and the number of branches and junctions (Fig. 7*B*) in Shunt PAEC indicative of a decrease in mitochondrial fission. Western blot analysis demonstrated that the NipR1-mediated decrease in mitochondrial fission in Shunt PAEC was associated with reduced RhoA nitration (Fig. 7*C*) and RhoA activity (Fig. 7*D*). NipR1 also reduced the p-S^{616} Drp1:Drp1 ratio (Fig. 7*E*). NipR1 increased the mitochondrial membrane potential (Fig. 7*F*) while mt-ROS (Fig. 7*G*) and HIF1α protein levels (Fig. 7*H*) were reduced. Moreover, the total cellular ATP production rate was increased (Fig. 7*I*). This was associated with decreased ATP generation from glycolysis (Fig. 7*J*). In contrast, ATP generation from oxidative phosphorylation (OXPHOS) was increased (Fig. 7*K*). Together, these data provide compelling evidence that nitration-mediated RhoA activation is essential for increasing mitochondrial fission and cellular glycolysis during PH development.

Discussion

Over the last decade, we, and others, have shown that, like cancer, the development of pulmonary vascular disease relies on metabolic reprogramming to favor glycolysis (22, 23, 26, 28, 30, 62–64). Furthermore, we have identified a causal link between this metabolic reprogramming and the development of the hyperproliferative endothelial phenotype in our lamb model of increased PBF (24). This link is, in part, because proliferating cells have different metabolic needs than non-proliferating cells (44); in addition to generating ATP, proliferating cells must also produce biosynthetic precursors such as nucleic acids and lipids required for cell division (45, 46). Transformed cells therefore frequently exhibit altered bioenergetic flux patterns. An example is aerobic glycolysis, wherein glucose is converted into lactate even under normoxic conditions (65, 66). Importantly, aerobic glycolysis has been observed in highly proliferative but nontransformed cells, including smooth muscle and endothelial cells in PH (25, 40). The work presented here adds to our knowledge of the mechanisms underlying this glycolytic switch in PH by identifying excess mitochondrial fission as an essential upstream event. Our data implicate increased HIF-1α signaling in the

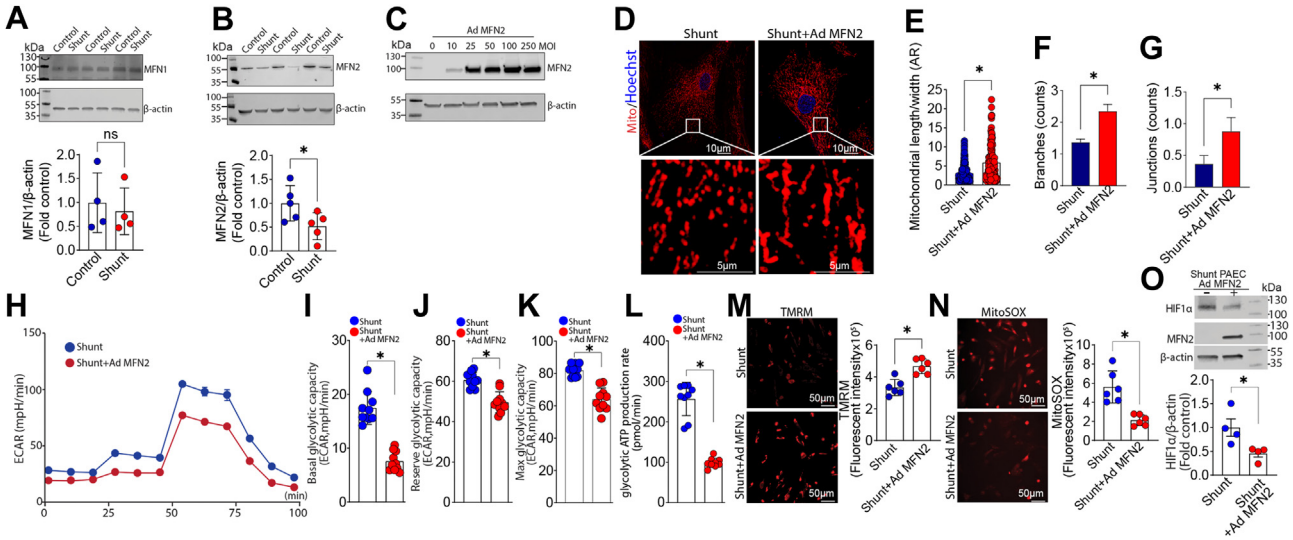

Figure 4. Overexpression of MFN2 attenuates mitochondrial fission and reduces cellular glycolysis in pulmonary arterial endothelial cells (PAECs) isolated from lambs with pulmonary hypertension. Western blot analysis was used to evaluate protein levels of MFN1 (*A*) and MFN2 (*B*) in PAEC isolated from Control and Shunt lambs. Although MFN1 levels are unchanged between Control- and Shunt-PAEC (*A*), MFN2 levels are significantly decreased in Shunt PAEC (*B*). Representative images are shown. β-Actin was used to normalize protein loading. Increasing MFN2 expression using an adenoviral construct (*C*) increases the aspect ratio (AR) and the number of mitochondrial branches and junctions in Shunt PAEC (*D–G*), indicative of increased mitochondrial fusion. Increasing MFN2 expression also attenuates cellular glycolysis (*H*) as evidenced by decreases in basal (*I*), reserve (*J*), and maximal (*K*) glycolytic capacity as well as reducing the glycolytic ATP production rate (*L*). Increasing MFN2 expression enhances the mitochondrial membrane potential in Shunt PAEC (*M*) and decreases mt-ROS levels (*N*). Western blot analysis shows that HIF1α protein levels are decreased (*O*). Representative images are shown. β-Actin was used to normalize protein loading. The scale bar represents 10 μm. Data are mean ± SE. *$p < 0.05$ *versus* Control PAEC or nontransduced Shunt PAEC.

glycolytic phenotype likely driven by increases in mt-ROS (24). HIF-1α upregulation is a characteristic of a proliferative cell phenotype and strongly links aerobic glycolysis to hyperproliferation in PH (67). In this study, we demonstrated that Shunt PAECs have a high level of basal glycolysis compared with PAECs isolated from Control lambs. This is reversed when mitochondrial fission is reduced either through Drp1 inhibition or overexpression of MFN2. Interestingly, we found that, in addition to Drp1 activation, MFN2 expression was decreased in Shunt PAEC. It is unclear how this occurs but is likely secondary to the increased mechanical forces that the endothelial layer is exposed to due to the presence of the aortopulmonary shunt *in vivo*. However, proteasomal degradation may be involved (68) since proteasomal activity is increased in Shunt lambs (69). Further studies will be required to evaluate this possibility. MFN-2 was initially known as "hyperplasia suppressor gene," due to its antiproliferative effect when overexpressed (70, 71). Thus, mitochondrial fusion is an underappreciated regulator of cell proliferation. Thus, the decrease in mitochondrial fusion is likely involved in endothelial cell hyperproliferation associated with PH *via* the modulation of cellular glycolysis. This possibility is supported by the fact that Shunt PAECs are hyperproliferative (72).

Mitochondria are present in a complex network structure that undergoes cycles of fission and fusion in response to various stimuli resulting in mitochondrial joining or

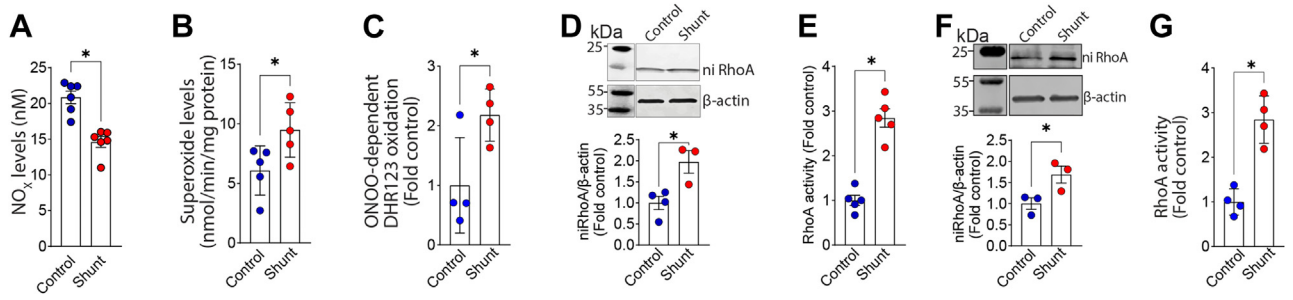

Figure 5. Increased oxidative and nitrative stress in pulmonary arterial endothelial cells (PAECs) isolated from lambs with pulmonary hypertension. NO_x levels were measured in PAEC isolated from Control and Shunt lambs (*A*). There is a decrease in NO_x levels in Shunt PAEC (*A*). Electron paramagnetic resonance analysis shows that superoxide levels are increased in Shunt PAEC (*B*). Peroxynitrite levels are also higher in Shunt PAEC, determined *via* the measurement of oxidation of dihydrorhodamine (DHR) 123 (*C*). Western blot analysis shows that RhoA nitration (ni-RhoA) is increased in Shunt PAEC (*D*). Representative images are shown. β-Actin was used to normalize protein loading. RhoA activity is also increased in Shunt PAEC (*E*). Western blot analysis shows that nitrated RhoA is increased in peripheral lung tissue prepared from 4-week-old Shunt-, compared with Control-lambs (*F*). Representative images are shown. β-Actin was used to normalize protein loading. RhoA activity also increases in peripheral lung tissue prepared from 4-week-old Shunt lambs (*G*). Data are mean ± SE. *$p < 0.05$ *versus* Control PAEC or Control lamb lung tissue.

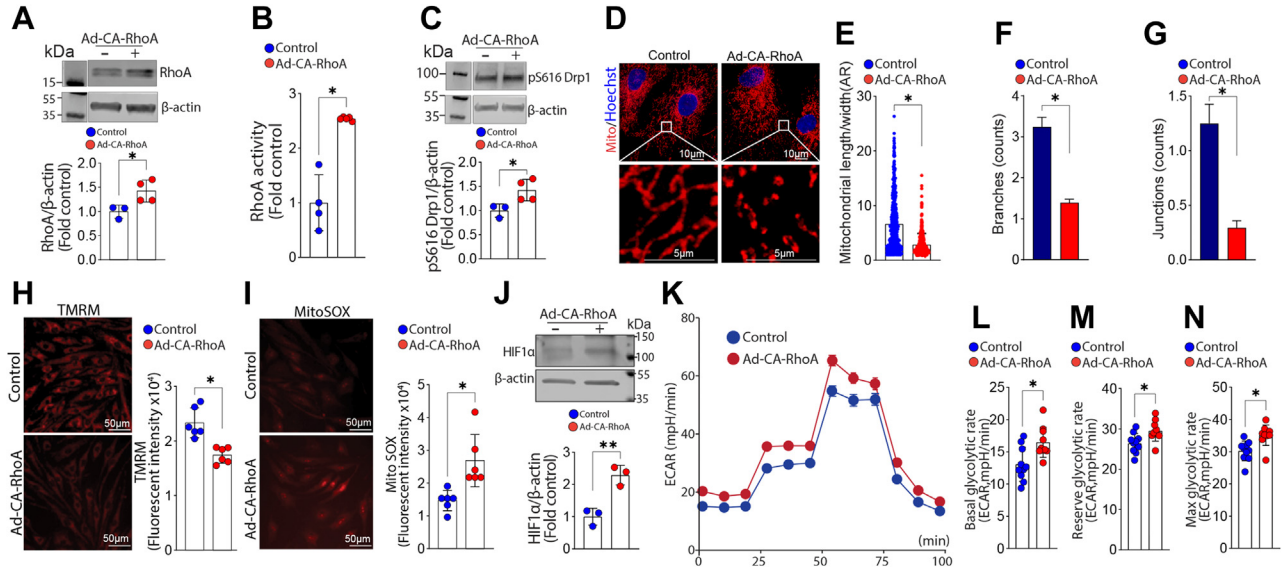

Figure 6. Increasing RhoA activity mimics a Shunt phenotype in pulmonary arterial endothelial cells (PAECs) isolated from Control lambs. PAECs isolated from Control lambs were transduced with an adenoviral construct expressing a constitutively active RhoA mutant (RhoAQ63L, CA-RhoA). Western blot analysis confirmed overexpression of RhoA (*A*). RhoA activity was also increased (*B*). Western blot analysis shows that pS^{616}Drp1 levels are increased in CA-RhoA expressing PAEC (*C*). The mitochondria were labeled with MitoTracker (*D*) were analyzed to evaluate changes in mitochondrial fission. There is a decrease in the aspect ratio (AR) (*E*) as well as the number of branches (*F*) and junctions (*G*) in CA-RhoA-expressing PAEC indicative of increased mitochondrial fission. The mitochondrial membrane potential decreases in CA-RhoA-expressing PAEC (*H*), and mt-ROS levels increase (*I*). Western blot analysis shows that HIF1α protein levels are increased in CA-RhoA-expressing PAEC (*J*). Representative Western blot images are shown. β-Actin was used to normalize protein loading. CA-RhoA overexpression also increases cellular glycolysis (*K*) as evidenced by increases in basal (*L*), reserve (*M*), and maximal (*N*) glycolytic capacity. The scale bar represents 10 μm. Data are mean ± SE. *$p < 0.05$ *versus* nontransduced PAEC.

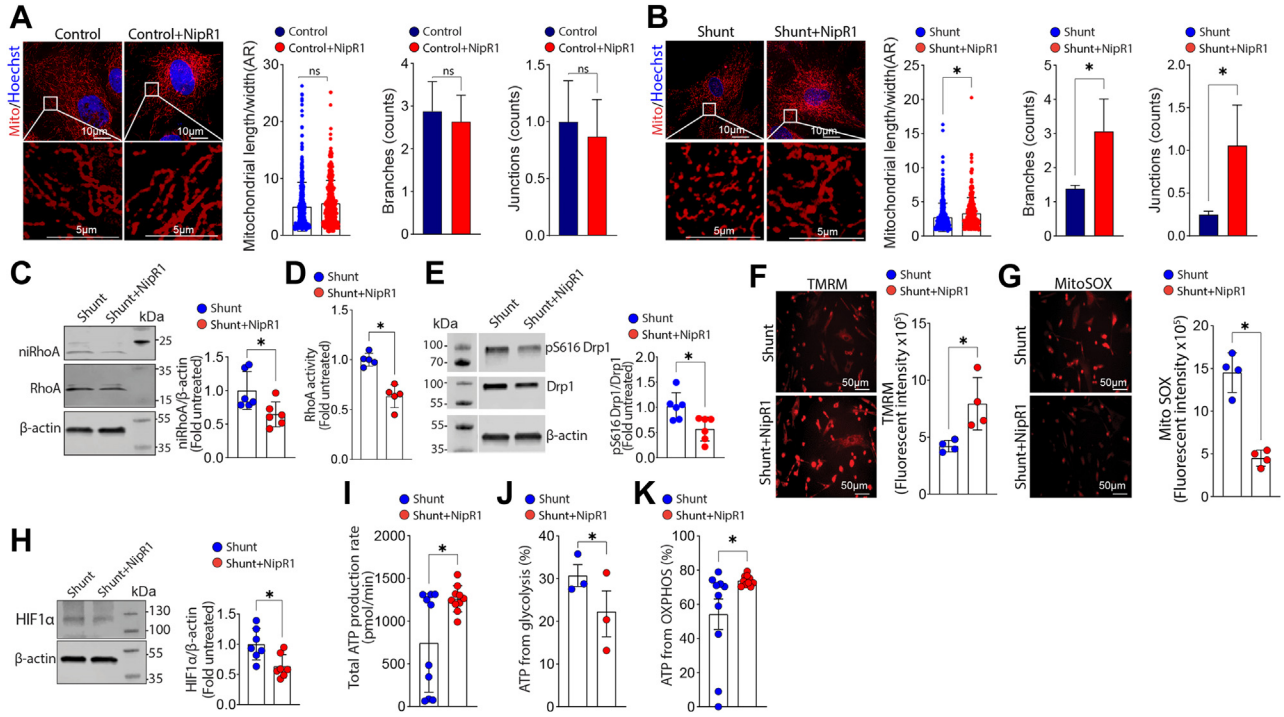

Figure 7. Decreasing nitrated RhoA levels reverses mitochondrial fission and reduces cellular glycolysis in pulmonary arterial endothelial cells (PAECs) isolated from lambs with pulmonary hypertension. PAECs were treated or not with the RhoA nitration shielding peptide, NipR1 (100 ng/ml, 24 h), then the mitochondria were labeled with MitoTracker, and effects on mitochondrial fission were analyzed. NipR1 exposure does not change the aspect ratio (AR), branches, and junctions counts in Control PAEC (*A*) but increases the AR and the number of mitochondrial branches and junctions in Shunt PAEC (*B*), indicative of increased mitochondrial fusion. Western blot analysis confirmed NipR1 decreased nitrated RhoA levels (ni-RhoA, *C*) and decreased RhoA activity (*D*) in Shunt PAEC. Western blot analysis also demonstrated that NipR1 decreased the pS^{616}Drp1:total Drp1 ratio (*E*). NipR1 increased the mitochondrial membrane potential (*F*) and decreased mt-ROS levels (*G*) in Shunt PAEC. Western blot analysis showed this correlated with decreased HIF1α levels (*H*). Representative Western blot images are shown. β-Actin was used to normalize protein loading. The total ATP production rate in Shunt PAEC cells was increased by NipR1 treatment (*I*). This was associated with a decrease in ATP derived from cellular glycolysis (*J*) and an increased ATP generated by oxidative phosphorylation (OXPHOS, *K*). The scale bar represents 10 μm. Data are mean ± SE. *$p < 0.05$ *versus* untreated Shunt PAEC.

separation, respectively. This process is regulated by several dynamin-like GTPases, including Drp1 (73). Fission involves the formation of Drp1 into helical oligomers on the outer mitochondrial membrane, which in turn causes membrane constriction and mitochondrial fragmentation (74, 75). An essential regulator of Drp1 activity is phosphorylation status. Phosphorylation at S^{616} activates Drp1 to promote mitochondrial fission (76, 77). Conversely, phosphorylation of Drp1 at S^{637} inhibits the mitochondrial fission (76, 77). Among the kinases known to phosphorylate, and activate, Drp1 is Rho-kinase (ROCK) (60, 61). ROCK exists as two isoforms, 1 and 2, and is a significant player in the development of pulmonary vascular disease through its ability to reorganize the actin cytoskeleton. One of the major upstream activators of ROCK is RhoA (Ras homologous GTP-binding protein A). The canonical activation of RhoA GTPase is induced through G protein–coupled receptors or tyrosine kinases in combination with guanine nucleotide exchange factors that stimulate the exchange of GDP for GTP and the translocation of GTP-RhoA to the plasma membrane. Upon translocation to the plasma membrane, GTP-RhoA activates ROCK. We recently identified a new mechanism of RhoA activation through a protein nitration event at Y^34 that stimulates RhoA nucleotide exchange, independent of guanine nucleotide exchange factors activation (58). Protein nitration events are enhanced in our Shunt lamb model of PH (50, 78, 79). Drp1 has been shown to be regulated by post-translational modifications other than phosphorylation including, very recently, nitration (80). Mass spectrometry analyses have identified two tyrosine (Y) sites susceptible to nitration at Y^{628} and Y^{665} (80). Both sites are in the C-terminal GTPase effector domain (GED) of Drp1. The GED regulates Drp1 GTPase activity and Drp1 oligomer/polymer formation (81). Nitration of these sites enhances Drp1 oligomer assembly rather than its GTPase activity (80). Thus, we speculate that Drp1 nitration may also be involved in the increased fission in Shunt PAEC; further studies will be required to evaluate this possibility.

Previous work in PH has focused on the role of RhoA-ROCK signaling as it relates to changes in vasoconstriction. For example, in a conditional ROCK2 knockout mouse, the increase in right ventricular systolic pressure in response to chronic hypoxia is blunted (82). Serum ROCK2 concentrations are significantly elevated in patients with PH (83) and the nonspecific ROCK inhibitor, fasudil, is beneficial in both animal models of PH (84–86) and in patients with PH (87). Interestingly, KD025, a ROCK2 inhibitor currently being tested in clinical trials, promotes OXPHOS and decreases glycolysis in pulmonary microvascular endothelial cells (88). The overexpression of a constitutively active isoform of RhoA induces mitochondrial fission and cellular glycolysis. Thus, the beneficial effects of ROCK inhibition may not be solely related to reductions in smooth muscle cell constriction. However, global, nonspecific, ROCK inhibition should be approached with caution. A prior study, using cardiac-specific ROCK1-deficient ($cROCK1^{-/-}$) and ROCK2-deficient ($cROCK2^{-/-}$) mice, found that loss of ROCK1 promoted pressure-overload-mediated cardiac dysfunction and postcapillary PH, whereas loss of ROCK2 had the opposite effect (89). Thus, an approach in which there are only targeted pathologic changes would be more desirable. Our data validate this approach using our novel shielding peptide, NipR1 (58). This peptide is designed to prevent the nitration of RhoA at Y^{34}, which we have shown to stimulate pathologic RhoA signaling (58, 59). Mechanistically, this involves enhanced GDP release and GTP reload (58). Not only does NipR1 treatment decrease mitochondrial fission induced cellular glycolysis but it also restores mitochondrial function and enhances OXPHOS. However, further studies using animal models of PH will be required to validate the utility of NipR1 as a therapy.

In conclusion, our studies reveal for the first time that increases in mitochondrial fission enhance a Warburg phenotype in PAEC. Furthermore, the increases in mitochondrial fission are dependent on changes in both the fission and fusion pathways. In addition, we have identified a novel mechanism that drives Drp1 activation through the nitration-mediated activation of RhoA at Y^{34} due to endothelial nitric oxide synthase uncoupling (Fig. 8). We speculate that preventing RhoA nitration Y^{34} could be a new therapy for PH and that our NipR1 peptide is a potential novel agent for PH.

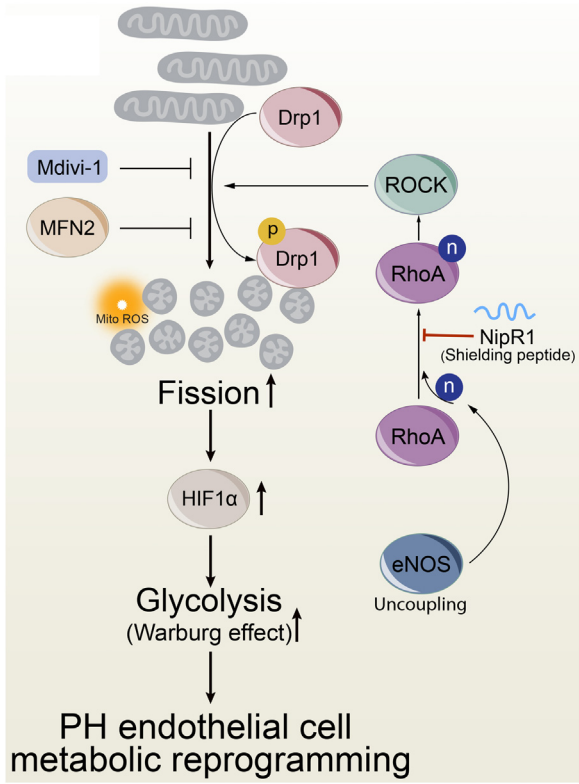

Figure 8. Schematic representation of enhanced mitochondrial fission–mediated glycolysis through nitration-mediated activation of RhoA. The increased cellular glycolysis (Warburg effect) in pulmonary hypertension (PH) is driven by increased Drp1-mediated mitochondrial fission and enhanced HIF-1α signaling. Drp1 is activated by phosphorylation at S616. Blocking Drp1 activity (Mdivi-1) or stimulating fusion (MFN2 overexpression) reduces aerobic glycolysis. Drp1 S616 phosphorylation is stimulated by the nitration-mediated activation of RhoA due to increased endothelial nitric oxide synthase uncoupling. Blocking the nitration of RhoA with NipR1 reduces Drp1 activity in PH pulmonary arterial endothelial cells; this decreases aerobic glycolysis and reverses the metabolic reprogramming.

Experimental procedures

Lamb model of pulmonary hypertension associated with increased PBF and pressure

The surgical protocol in which an 8-mm Gore-Tex vascular graft, ~2 mm in length, is anastomosed between the ascending aorta and main pulmonary artery in anesthetized late-gestation fetal lambs (137–141 days gestation) was carried out as described (52). Lambs were sacrificed 4 weeks after spontaneous delivery (49). All animal protocols and procedures were approved by the Committees on Animal Research of the University of California, San Francisco (protocol number AN196124).

Cell culture and measurement

Primary cultures of ovine PAEC were isolated and cultured from ten 4-week-old Shunt and control lambs including three pairs of twin lambs as described (90, 91). NO_x levels were determined in cell culture medium using a Sievers 280i Nitric Oxide Analyzer (GE Analytical) as described (49). Results were analyzed using the Liquid software (GE), and the resultant NO_x value represents total NO and nitrite. For the measurement of superoxide generation, electron paramagnetic resonance was performed as described (92). To detect the level of cell peroxynitrite levels, the oxidation of dihydrorhodamine 123 (EMD Millipore) to rhodamine 123, in the presence of PEG-Catalase (100 U), was measured as we have described (79).

Adenoviral-mediated expression

A constitutively active RhoA mutant, prepared by introducing a Q63L mutation into the wildtype RhoA sequence, was a generous gift from David Fulton (Augusta University). Ad-MFN1 was purchased commercially (Vector Biolabs). Viruses were titered using a commercial Kit (Takara Bio) according to the manufacturer's instructions. PAECs were infected as described (93) using a multiplicity of infection = 100. Cells were analyzed 48 h post infection.

Western blot analysis

Western blotting was performed using 4 to 20% SDS-polyacrylamide gels (Bio-Rad), transferred to polyvinylidene difluoride membranes (Bio-Rad). Reactive bands in the membranes were detected using the following antibodies: pS616Drp1, Drp1, and RhoA all from Cell Signaling Technology HIF-1α from Novus; and MFN1 and MFN2 from Abcam. The antibody specific to RhoA nitrated at Y^{34} was generated as described (94). Protein bands were visualized using the Super Signal West Femto chemiluminescence kit (Pierce). Bands were quantified using LI-COR Image Station software. Membranes were reprobed with a β-actin-specific antibody to normalize loading (Sigma).

RhoA activity

RhoA activity was detected by the Rhotekin Rho-binding domain pulldown assay (Cell Signaling Technology) using the manufacturers protocol. The level of active RhoA was measured using Western blot analysis.

Peptide synthesis

The NipR1 peptide containing the amino acid sequence 31 to 39 of RhoA fused with the cell-permeable TAT sequence was synthesized by Peptide 2.0 Inc. NipR1 has been shown to specifically block RhoA nitration (58, 59).

Mitochondrial bioenergetics

Mitochondrial bioenergetics were evaluated using the XF Cell Mito Stress Test Kit in combination with a XF24 Analyzer (both from Seahorse Biosciences) as described (90).

Cellular ATP rate analysis

To estimate changes in cellular total ATP production rates and the ATP generated from mitochondrial OXPHOS or cellular glycolysis we utilized an XF Real-Time ATP Rate Kit (Seahorse Bioscience) in combination with a Seahorse XF24 analyzer according to the manufacturers guidelines. The mitochondrial ATP production rate is calculated according to the equation: OCRATP (pmol/min)*2(pmol O/pmolO2)*P/O (pmol ATP/pmol O). The glycolytic ATP production rate is calculated using the glycolytic proton efflux rate.

Fluorescent detection of mitochondrial membrane potential and mitochondrial ROS

Mitochondrial membrane potential was determined using tetramethylrhodamine methyl ester perchlorate, TMRM (#I34361, ThermoFisher) and mt-ROS using MitoSOX Red mitochondrial superoxide indicator (#M36008, ThermoFisher) using an Olympus IX51 microscope equipped with a CCD camera (Hamamatsu Photonics) for the acquisition of fluorescent images as described (90). Average fluorescent intensities (to correct for differences in cell number) were quantified using ImagePro Plus imaging software (Media Cybernetics).

Analysis of mitochondrial fission

Cells were labeled with 30 nM MitoTracker (#M7512, Invitrogen) for 15 min at 37 °C; Hoechst 33342 (# R37605, ThermoFisher) was used for nuclei staining. Low-noise and high-sensitivity fluorescence images were then captured using a KEYENCE BZ-X800 fluorescence microscope ×60 objective. Mitochondrial fission morphology analysis was performed using ImageJ/FiJi (NIH). The mitochondrial long axis and wide axis were measured by particle analysis measurement. The aspect ratio was calculated to represent the mitochondrial fragmentation characteristics (95–97). Binary images were also prepared for skeleton analysis using the ImageJ/FiJi plugin MiNA (98).

Immunofluorescence microscopy

Cells on coverslips were fixed with 4% paraformaldehyde (#47608, Sigma-Aldrich) for 30 min at room temperature.

Cells were permeabilized with 0.25% Triton X-100 in PBS for 30 min at room temperature and incubated in 1% bovine serum albumin (PBS +0.1% Tween20) to block nonspecific antibody binding (1 h, at room temperature). TOMM20 antibody (#PA5-52843, ThermoFisher, 1:200), phospho-Drp1 (Ser616) (#3455S, Cell Signaling Technology, 1:200), and Drp1 antibody (#5391S, Cell Signaling Technology, 1:200) were incubated either at 4 °C, in a humidified chamber overnight, or at room temperature for 1 h, then incubation with a secondary antibody in 1% bovine serum albumin, for 1 h at room temperature in the dark. The nuclei were then stained using NucBlue probe (#R37605, ThermoFisher). Slides were then mounted with ProLong Glass Antifade Mountant (Invitrogen, ThermoFisher) for observation. The preceding steps were carried out in the dark. Cell images were acquired using Nikon Eclipse TE2000-U microscope, with Hamamatsu digital camera C11440, using an ×100 objective, and fluorescent images were captured with software NIS-Elements (Nikon). The images were processed and analyzed for colocalization correlation with ImagePro Plus 7.0 system (Media Cybernetics) or ImageJ (NIH).

Statistical analysis

GraphPad Prism (GraphPad Software, version 9) was used for statistical analyses. In each experiment we calculated the mean ± SEM. The unpaired *t* test was used to calculate statistical significance. Any individual data sample greater than two SD from the mean was excluded from analysis. A $p < 0.05$ was used to determine significance.

Data availability

The data that support the findings of this study are available from the corresponding author upon reasonable request.

Author contributions—J. R. F., T. W., and S. M. B. conceptualization; Q. L. and S. M. B. data curation; Q. L., X. S., M. Y., W. O., X. W., H. W., A. G.-F., V. D. S., and E. A. Z. methodology; Q. L. writing-original draft; E. A. Z., K. T., J. R. F., T. W., and S. M. B. writing-review and editing; J. R. F., T. W., and S. M. B. resources; S. M. B. supervision; S. M. B. project administration.

Funding and additional information—This research was supported in part by HL60190 (S. M. B.), HL137282 (S. M. B./J. R. F.), HL134610 (S. M. B./T. W./E. A. Z.), HL142212 (S. M. B./E. A. Z.), HL146369 (S. M. B./T. W./J. R. F.), and the Interdisciplinary Training in Cardiovascular Research T32 HL007249 (to X. W.) all from the National Institutes of Health. The content is solely the responsibility of the authors and does not necessarily represent the official views of the National Institutes of Health.

Conflict of interest—The authors declare they have no conflicts of interest with the contents of this article.

Abbreviations—The abbreviations used are: Drp1, dynamin-related protein 1; mt-ROS, mitochondrial reactive oxygen species; OXPHOS, oxidative phosphorylation; PAEC, pulmonary arterial endothelial cell; PBF, pulmonary blood flow; PH, pulmonary hypertension; PVD, pulmonary vascular disease; ROCK, Rho-kinase.

References

1. Burrows, F. A., Klinck, J. R., Rabinovitch, M., and Bohn, D. J. (1986) Pulmonary hypertension in children: perioperative management. *Can. Anaesth. Soc. J.* **33**, 606–628
2. Hoffman, J. I., Rudolph, A. M., and Heymann, M. A. (1981) Pulmonary vascular disease with congenital heart lesions: pathologic features and causes. *Circulation* **64**, 873–877
3. Kouchoukos, N. T., Blackstone, E. H., and Kirklin, J. W. (1978) Surgical implications of pulmonary hypertension in congenital heart disease. *Adv. Cardiol.*, 225–231
4. Meyrick, B., and Reid, L. (1980) Ultrastructural findings in lung biopsy material from children with congenital heart defects. *Am. J. Pathol.* **101**, 527–542
5. Rabinovitch, M., Haworth, S. G., Castaneda, A. R., Nadas, A. S., and Reid, L. M. (1978) Lung biopsy in congenital heart disease: a morphometric approach to pulmonary vascular disease. *Circulation* **58**, 1107–1122
6. Reid, L. M. (1986) Structure and function in pulmonary hypertension. New perceptions. *Chest* **89**, 279–288
7. Reid, L. M. (1979) The pulmonary circulation: remodeling in growth and disease. The 1978 J. Burns Amberson lecture. *Am. Rev. Respir. Dis.* **119**, 531–546
8. Rabinovitch, M., Keane, J. F., Norwood, W. I., Castaneda, A. R., and Reid, L. (1984) Vascular structure in lung tissue obtained at biopsy correlated with pulmonary hemodynamic findings after repair of congenital heart defects. *Circulation* **69**, 655–667
9. Haworth, S. G., and Reid, L. (1977) Quantitative structural study of pulmonary circulation in the newborn with aortic atresia, stenosis, or coarctation. *Thorax* **32**, 121–128
10. Haworth, S. G. (1984) Pulmonary vascular disease in different types of congenital heart disease. Implications for interpretation of lung biopsy findings in early childhood. *Br. Heart J.* **52**, 557–571
11. Hislop, A., Haworth, S. G., Shinebourne, E. A., and Reid, L. (1975) Quantitative structural analysis of pulmonary vessels in isolated ventricular septal defect in infancy. *Br. Heart J.* **37**, 1014–1021
12. Heath, D., and Edwards, J. E. (1958) The pathology of hypertensive pulmonary vascular disease; a description of six grades of structural changes in the pulmonary arteries with special reference to congenital cardiac septal defects. *Circulation* **18**, 533–547
13. Celermajer, D. S., Cullen, S., and Deanfield, J. E. (1993) Impairment of endothelium-dependent pulmonary artery relaxation in children with congenital heart disease and abnormal pulmonary hemodynamics. *Circulation* **87**, 440–446
14. Black, S., Fineman, J., Johengen, M., Bristow, J., and Soifer, S. (1998) Increased pulmonary blood flow alters the molecular regulation of vascular reactivity in the lamb. *Chest* **114**, 39S
15. Black, S. M., Bekker, J. M., McMullan, D. M., Parry, A. J., Ovadia, B., Reinhartz, O., *et al.* (2002) Alterations in nitric oxide production in 8-week-old lambs with increased pulmonary blood flow. *Pediatr. Res.* **52**, 233–244
16. Black, S. M., Sanchez, L. S., Mata-Greenwood, E., Bekker, J. M., Steinhorn, R. H., and Fineman, J. R. (2001) sGC and PDE5 are elevated in lambs with increased pulmonary blood flow and pulmonary hypertension. *Am. J. Physiol. Lung Cell Mol. Physiol.* **281**, L1051–L1057
17. Reddy, V. M., Wong, J., Liddicoat, J. R., Johengen, M., Chang, R., and Fineman, J. R. (1996) Altered endothelium-dependent responses in lambs with pulmonary hypertension and increased pulmonary blood flow. *Am. J. Physiol.* **271**, H562–570
18. Steinhorn, R. H., Russell, J. A., Lakshminrusimha, S., Gugino, S. F., Black, S. M., and Fineman, J. R. (2001) Altered endothelium-dependent relaxations in lambs with high pulmonary blood flow and pulmonary hypertension. *Am. J. Physiol. Heart Circ. Physiol.* **280**, H311–H317
19. Tworetzky, W., Moore, P., Bekker, J. M., Bristow, J., Black, S. M., and Fineman, J. R. (2000) Pulmonary blood flow alters nitric oxide production

in patients undergoing device closure of atrial septal defects. *J. Am. Coll. Cardiol.* **35**, 463–467
20. Chan, S. Y., and Rubin, L. J. (2017) Metabolic dysfunction in pulmonary hypertension: from basic science to clinical practice. *Eur. Respir. Rev.* **26**, 170094
21. Yu, Q., and Chan, S. Y. (2017) Mitochondrial and metabolic drivers of pulmonary vascular endothelial dysfunction in pulmonary hypertension. *Adv. Exp. Med. Biol.* **967**, 373–383
22. Rafikova, O., Meadows, M. L., Kinchen, J. M., Mohney, R. P., Maltepe, E., Desai, A. A., *et al.* (2016) Metabolic changes precede the development of pulmonary hypertension in the monocrotaline exposed rat lung. *PLoS One* **11**, e0150480
23. Rafikov, R., Sun, X., Rafikova, O., Meadows, M. L., Desai, A. A., Khalpey, Z., *et al.* (2015) Complex I dysfunction underlies the glycolytic switch in pulmonary hypertensive smooth muscle cells. *Redox Biol.* **6**, 278–286
24. Sun, X., Kumar, S., Sharma, S., Aggarwal, S., Lu, Q., Gross, C., *et al.* (2014) Endothelin-1 induces a glycolytic switch in pulmonary arterial endothelial cells via the mitochondrial translocation of endothelial nitric oxide synthase. *Am. J. Respir. Cell Mol. Biol.* **50**, 1084–1095
25. Ryan, J. J., and Archer, S. L. (2015) Emerging concepts in the molecular basis of pulmonary arterial hypertension: part I: metabolic plasticity and mitochondrial dynamics in the pulmonary circulation and right ventricle in pulmonary arterial hypertension. *Circulation* **131**, 1691–1702
26. Archer, S. L. (2017) Pyruvate kinase and Warburg metabolism in pulmonary arterial hypertension: uncoupled glycolysis and the cancer-like phenotype of pulmonary arterial hypertension. *Circulation* **136**, 2486–2490
27. Chen, Z., Liu, M., Li, L., and Chen, L. (2018) Involvement of the Warburg effect in non-tumor diseases processes. *J. Cell Physiol.* **233**, 2839–2849
28. Liu, N., Parry, S., Xiao, Y., Zhou, S., and Liu, Q. (2017) Molecular targets of the Warburg effect and inflammatory cytokines in the pathogenesis of pulmonary artery hypertension. *Clin. Chim. Acta* **466**, 98–104
29. Zhang, R., and Jing, Z. C. (2016) Energetic metabolic roles in pulmonary arterial hypertension and right ventricular remodeling. *Curr. Pharm. Des.* **22**, 4780–4795
30. Peng, H., Xiao, Y., Deng, X., Luo, J., Hong, C., and Qin, X. (2016) The Warburg effect: a new story in pulmonary arterial hypertension. *Clin. Chim. Acta* **461**, 53–58
31. Hansen, T., Galougahi, K. K., Celermajer, D., Rasko, N., Tang, O., Bubb, K. J., *et al.* (2016) Oxidative and nitrosative signalling in pulmonary arterial hypertension - implications for development of novel therapies. *Pharmacol. Ther.* **165**, 50–62
32. Cottrill, K. A., and Chan, S. Y. (2013) Metabolic dysfunction in pulmonary hypertension: the expanding relevance of the Warburg effect. *Eur. J. Clin. Invest.* **43**, 855–865
33. Chiong, M., Morales, P., Torres, G., Gutierrez, T., Garcia, L., Ibacache, M., *et al.* (2013) Influence of glucose metabolism on vascular smooth muscle cell proliferation. *Vasa* **42**, 8–16
34. Rabinovitch, M. (2012) Molecular pathogenesis of pulmonary arterial hypertension. *J. Clin. Invest.* **122**, 4306–4313
35. Rich, S. (2012) Right ventricular adaptation and maladaptation in chronic pulmonary arterial hypertension. *Cardiol. Clin.* **30**, 257–269
36. Xu, W., and Erzurum, S. C. (2011) Endothelial cell energy metabolism, proliferation, and apoptosis in pulmonary hypertension. *Compr. Physiol.* **1**, 357–372
37. Bonnet, S., Archer, S. L., Allalunis-Turner, J., Haromy, A., Beaulieu, C., Thompson, R., *et al.* (2007) A mitochondria-K+ channel axis is suppressed in cancer and its normalization promotes apoptosis and inhibits cancer growth. *Cancer Cell* **11**, 37–51
38. Haddad, F., Ashley, E., and Michelakis, E. D. (2010) New insights for the diagnosis and management of right ventricular failure, from molecular imaging to targeted right ventricular therapy. *Curr. Opin. Cardiol.* **25**, 131–140
39. Michelakis, E. D., Gurtu, V., Webster, L., Barnes, G., Watson, G., Howard, L., *et al.* (2017) Inhibition of pyruvate dehydrogenase kinase improves pulmonary arterial hypertension in genetically susceptible patients. *Sci. Transl. Med.* **9**, eaao4583
40. Paulin, R., and Michelakis, E. D. (2014) The metabolic theory of pulmonary arterial hypertension. *Circ. Res.* **115**, 148–164
41. Sutendra, G., Bonnet, S., Rochefort, G., Haromy, A., Folmes, K. D., Lopaschuk, G. D., *et al.* (2010) Fatty acid oxidation and malonyl-CoA decarboxylase in the vascular remodeling of pulmonary hypertension. *Sci. Transl. Med.* **2**, 44ra58
42. Sutendra, G., Dromparis, P., Paulin, R., Zervopoulos, S., Haromy, A., Nagendran, J., *et al.* (2013) A metabolic remodeling in right ventricular hypertrophy is associated with decreased angiogenesis and a transition from a compensated to a decompensated state in pulmonary hypertension. *J. Mol. Med. (Berl.)* **91**, 1315–1327
43. Sutendra, G., and Michelakis, E. D. (2014) The metabolic basis of pulmonary arterial hypertension. *Cell Metab.* **19**, 558–573
44. Vander Heiden, M. G., Cantley, L. C., and Thompson, C. B. (2009) Understanding the Warburg effect: the metabolic requirements of cell proliferation. *Science* **324**, 1029–1033
45. Kilburn, D. G., Lilly, M. D., and Webb, F. C. (1969) The energetics of mammalian cell growth. *J. Cell Sci.* **4**, 645–654
46. Locasale, J. W., and Cantley, L. C. (2011) Metabolic flux and the regulation of mammalian cell growth. *Cell Metab.* **14**, 443–451
47. Boehme, J., Sun, X., Tormos, K. V., Gong, W., Kellner, M., Datar, S. A., *et al.* (2016) Pulmonary artery smooth muscle cell hyperproliferation and metabolic shift triggered by pulmonary overcirculation. *Am. J. Physiol. Heart Circ. Physiol.* **311**, H944–H957
48. Sharma, S., Barton, J., Rafikov, R., Aggarwal, S., Kuo, H. C., Oishi, P. E., *et al.* (2013) Chronic inhibition of PPAR-gamma signaling induces endothelial dysfunction in the juvenile lamb. *Pulm. Pharmacol. Ther.* **26**, 271–280
49. Sharma, S., Aramburo, A., Rafikov, R., Sun, X., Kumar, S., Oishi, P. E., *et al.* (2013) L-carnitine preserves endothelial function in a lamb model of increased pulmonary blood flow. *Pediatr. Res.* **74**, 39–47
50. Sharma, S., Sud, N., Wiseman, D. A., Carter, A. L., Kumar, S., Hou, Y., *et al.* (2008) Altered carnitine homeostasis is associated with decreased mitochondrial function and altered nitric oxide signaling in lambs with pulmonary hypertension. *Am. J. Physiol. Lung Cell Mol. Physiol.* **294**, L46–L56
51. Mata-Greenwood, E., Meyrick, B., Steinhorn, R. H., Fineman, J. R., and Black, S. M. (2003) Alterations in TGF-beta1 expression in lambs with increased pulmonary blood flow and pulmonary hypertension. *Am. J. Physiol. Lung Cell Mol. Physiol.* **285**, L209–221
52. Reddy, V. M., Meyrick, B., Wong, J., Khoor, A., Liddicoat, J. R., Hanley, F. L., *et al.* (1995) In utero placement of aortopulmonary shunts. A model of postnatal pulmonary hypertension with increased pulmonary blood flow in lambs. *Circulation* **92**, 606–613
53. Cerveny, K. L., Tamura, Y., Zhang, Z., Jensen, R. E., and Sesaki, H. (2007) Regulation of mitochondrial fusion and division. *Trends Cell Biol.* **17**, 563–569
54. Hall, A. R., Burke, N., Dongworth, R. K., and Hausenloy, D. J. (2014) Mitochondrial fusion and fission proteins: novel therapeutic targets for combating cardiovascular disease. *Br. J. Pharmacol.* **171**, 1890–1906
55. Macdonald, P. J., Stepanyants, N., Mehrotra, N., Mears, J. A., Qi, X., Sesaki, H., *et al.* (2014) A dimeric equilibrium intermediate nucleates Drp1 reassembly on mitochondrial membranes for fission. *Mol. Biol. Cell* **25**, 1905–1915
56. Ryan, J., Dasgupta, A., Huston, J., Chen, K. H., and Archer, S. L. (2015) Mitochondrial dynamics in pulmonary arterial hypertension. *J. Mol. Med. (Berl.)* **93**, 229–242
57. Chen, K. H., Dasgupta, A., Lin, J., Potus, F., Bonnet, S., Iremonger, J., *et al.* (2018) Epigenetic dysregulation of the dynamin-related protein 1 binding partners MiD49 and MiD51 increases mitotic mitochondrial fission and promotes pulmonary arterial hypertension: mechanistic and therapeutic implications. *Circulation* **138**, 287–304
58. Rafikov, R., Dimitropoulou, C., Aggarwal, S., Kangath, A., Gross, C., Pardo, D., *et al.* (2014) Lipopolysaccharide-induced lung injury involves the nitration-mediated activation of RhoA. *J. Biol. Chem.* **289**, 4710–4722
59. Wang, H., Sun, X., Lu, Q., Zemskov, E. A., Yegambaram, M., Wu, X., *et al.* (2021) The mitochondrial redistribution of eNOS is involved in

lipopolysaccharide induced inflammasome activation during acute lung injury. *Redox Biol.* **41**, 101878
60. Brand, C. S., Tan, V. P., Brown, J. H., and Miyamoto, S. (2018) RhoA regulates Drp1 mediated mitochondrial fission through ROCK to protect cardiomyocytes. *Cell Signal.* **50**, 48–57
61. Martorell-Riera, A., Segarra-Mondejar, M., Reina, M., Martinez-Estrada, O. M., and Soriano, F. X. (2015) Mitochondrial fragmentation in excitotoxicity requires ROCK activation. *Cell Cycle* **14**, 1365–1369
62. Fijalkowska, I., Xu, W., Comhair, S. A., Janocha, A. J., Mavrakis, L. A., Krishnamachary, B., *et al.* (2010) Hypoxia inducible-factor1alpha regulates the metabolic shift of pulmonary hypertensive endothelial cells. *Am. J. Pathol.* **176**, 1130–1138
63. Xu, W., Koeck, T., Lara, A. R., Neumann, D., DiFilippo, F. P., Koo, M., *et al.* (2007) Alterations of cellular bioenergetics in pulmonary artery endothelial cells. *Proc. Natl. Acad. Sci. U. S. A.* **104**, 1342–1347
64. Archer, S. L., Fang, Y. H., Ryan, J. J., and Piao, L. (2013) Metabolism and bioenergetics in the right ventricle and pulmonary vasculature in pulmonary hypertension. *Pulm. Circ.* **3**, 144–152
65. Sciacovelli, M., Gaude, E., Hilvo, M., and Frezza, C. (2014) The metabolic alterations of cancer cells. *Methods Enzymol.* **542**, 1–23
66. Dang, C. V., Hamaker, M., Sun, P., Le, A., and Gao, P. (2011) Therapeutic targeting of cancer cell metabolism. *J. Mol. Med. (Berl.)* **89**, 205–212
67. Wang, Z., Yang, K., Zheng, Q., Zhang, C., Tang, H., Babicheva, A., *et al.* (2019) Divergent changes of p53 in pulmonary arterial endothelial and smooth muscle cells involved in the development of pulmonary hypertension. *Am. J. Physiol. Lung Cell Mol. Physiol.* **316**, L216–L228
68. Dasgupta, A., Chen, K. H., Lima, P. D. A., Mewburn, J., Wu, D., Al-Qazazi, R., *et al.* (2021) PINK1-induced phosphorylation of mitofusin 2 at serine 442 causes its proteasomal degradation and promotes cell proliferation in lung cancer and pulmonary arterial hypertension. *FASEB J.* **35**, e21771
69. Sun, X., Fratz, S., Sharma, S., Hou, Y., Rafikov, R., Kumar, S., *et al.* (2011) C-terminus of heat shock protein 70-interacting protein-dependent GTP cyclohydrolase I degradation in lambs with increased pulmonary blood flow. *Am. J. Respir. Cell Mol. Biol.* **45**, 163–171
70. Chen, H., and Chan, D. C. (2005) Emerging functions of mammalian mitochondrial fusion and fission. *Hum. Mol. Genet.* **15**, R283–289
71. Chan, D. C. (2006) Mitochondrial fusion and fission in mammals. *Annu. Rev. Cell Dev. Biol.* **22**, 79–99
72. Johnson Kameny, R., Datar, S. A., Boehme, J. B., Morris, C., Zhu, T., Goudy, B. D., *et al.* (2019) Ovine models of congenital heart disease and the consequences of hemodynamic alterations for pulmonary artery remodeling. *Am. J. Respir. Cell Mol. Biol.* **60**, 503–514
73. Kraus, F., Roy, K., Pucadyil, T. J., and Ryan, M. T. (2021) Function and regulation of the divisome for mitochondrial fission. *Nature* **590**, 57–66
74. Kamerkar, S. C., Kraus, F., Sharpe, A. J., Pucadyil, T. J., and Ryan, M. T. (2018) Dynamin-related protein 1 has membrane constricting and severing abilities sufficient for mitochondrial and peroxisomal fission. *Nat. Commun.* **9**, 5239
75. Rosenbloom, A. B., Lee, S. H., To, M., Lee, A., Shin, J. Y., and Bustamante, C. (2014) Optimized two-color super resolution imaging of Drp1 during mitochondrial fission with a slow-switching Dronpa variant. *Proc. Natl. Acad. Sci. U. S. A.* **111**, 13093–13098
76. Santel, A., and Frank, S. (2008) Shaping mitochondria: the complex posttranslational regulation of the mitochondrial fission protein DRP1. *IUBMB Life* **60**, 448–455
77. Jahani-Asl, A., and Slack, R. S. (2007) The phosphorylation state of Drp1 determines cell fate. *EMBO Rep.* **8**, 912–913
78. Oishi, P. E., Wiseman, D. A., Sharma, S., Kumar, S., Hou, Y., Datar, S. A., *et al.* (2008) Progressive dysfunction of nitric oxide synthase in a lamb model of chronically increased pulmonary blood flow: a role for oxidative stress. *Am. J. Physiol. Lung Cell Mol. Physiol.* **295**, L756–L766
79. Aggarwal, S., Gross, C. M., Kumar, S., Datar, S., Oishi, P., Kalkan, G., *et al.* (2011) Attenuated vasodilatation in lambs with endogenous and exogenous activation of cGMP signaling: role of protein kinase G nitration. *J. Cell Physiol.* **226**, 3104–3113
80. Li, W., Feng, J., Gao, C., Wu, M., Du, Q., Tsoi, B., *et al.* (2019) Nitration of Drp1 provokes mitophagy activation mediating neuronal injury in experimental autoimmune encephalomyelitis. *Free Radic. Biol. Med.* **143**, 70–83
81. Zhu, P. P., Patterson, A., Stadler, J., Seeburg, D. P., Sheng, M., and Blackstone, C. (2004) Intra- and intermolecular domain interactions of the C-terminal GTPase effector domain of the multimeric dynamin-like GTPase Drp1. *J. Biol. Chem.* **279**, 35967–35974
82. Shimizu, T., Fukumoto, Y., Tanaka, S., Satoh, K., Ikeda, S., and Shimokawa, H. (2013) Crucial role of ROCK2 in vascular smooth muscle cells for hypoxia-induced pulmonary hypertension in mice. *Arterioscler. Thromb. Vasc. Biol.* **33**, 2780–2791
83. Liu, B., Chang, R., Duan, Z., Zhang, X., Shen, Y., Liu, X., *et al.* (2018) The level of ROCK1 and ROCK2 in patients with pulmonary hypertension in plateau area. *Sci. Rep.* **8**, 9356
84. Liu, P., Huang, W., Ding, Y., Wu, J., Liang, Z., Huang, Z., *et al.* (2021) Fasudil dichloroacetate alleviates SU5416/hypoxia-induced pulmonary arterial hypertension by ameliorating dysfunction of pulmonary arterial smooth muscle cells. *Drug Des. Devel. Ther.* **15**, 1653–1666
85. Sun, X. Z., Li, S. Y., Tian, X. Y., Hong, Z., and Li, J. X. (2019) Effect of Rho kinase inhibitor fasudil on the expression ET-1 and NO in rats with hypoxic pulmonary hypertension. *Clin. Hemorheol. Microcirc.* **71**, 3–8
86. Qi, L., Lv, T., Cheng, Y., Yu, M., Han, H., Kong, H., *et al.* (2019) Fasudil dichloroacetate (FDCA), an orally available agent with potent therapeutic efficiency on monocrotaline-induced pulmonary arterial hypertension rats. *Bioorg. Med. Chem. Lett.* **29**, 1812–1818
87. Fujita, H., Fukumoto, Y., Saji, K., Sugimura, K., Demachi, J., Nawata, J., *et al.* (2010) Acute vasodilator effects of inhaled fasudil, a specific Rho-kinase inhibitor, in patients with pulmonary arterial hypertension. *Heart Vessels* **25**, 144–149
88. Lee, J. Y., Stevens, R. P., Kash, M., Zhou, C., Koloteva, A., Renema, P., *et al.* (2020) KD025 Shifts pulmonary endothelial cell bioenergetics and decreases baseline lung permeability. *Am. J. Respir. Cell Mol. Biol.* **63**, 519–530
89. Sunamura, S., Satoh, K., Kurosawa, R., Ohtsuki, T., Kikuchi, N., Elias-Al-Mamun, M., *et al.* (2018) Different roles of myocardial ROCK1 and ROCK2 in cardiac dysfunction and postcapillary pulmonary hypertension in mice. *Proc. Natl. Acad. Sci. U. S. A.* **115**, E7129–E7138
90. Sun, X., Lu, Q., Yegambaram, M., Kumar, S., Qu, N., Srivastava, A., *et al.* (2020) TGF-beta1 attenuates mitochondrial bioenergetics in pulmonary arterial endothelial cells via the disruption of carnitine homeostasis. *Redox Biol.* **36**, 101593
91. Sharma, S., Sun, X., Kumar, S., Rafikov, R., Aramburo, A., Kalkan, G., *et al.* (2012) Preserving mitochondrial function prevents the proteasomal degradation of GTP cyclohydrolase I. *Free Radic. Biol. Med.* **53**, 216–229
92. Sun, X., Sharma, S., Fratz, S., Kumar, S., Rafikov, R., Aggarwal, S., *et al.* (2013) Disruption of endothelial cell mitochondrial bioenergetics in lambs with increased pulmonary blood flow. *Antioxid. Redox Signal.* **18**, 1739–1752
93. Kumar, S., Sun, X., Noonepalle, S. K., Lu, Q., Zemskov, E., Wang, T., *et al.* (2017) Hyper-activation of pp60(Src) limits nitric oxide signaling by increasing asymmetric dimethylarginine levels during acute lung injury. *Free Radic. Biol. Med.* **102**, 217–228
94. Gross, C. M., Rafikov, R., Kumar, S., Aggarwal, S., Ham, P. B., 3rd, Meadows, M. L., *et al.* (2015) Endothelial nitric oxide synthase deficient mice are protected from lipopolysaccharide induced acute lung injury. *PLoS One* **10**, e0119918
95. Rocha, A. G., Franco, A., Krezel, A. M., Rumsey, J. M., Alberti, J. M., Knight, W. C., *et al.* (2018) MFN2 agonists reverse mitochondrial defects in preclinical models of Charcot-Marie-Tooth disease type 2A. *Science* **360**, 336–341
96. Delmotte, P., Marin Mathieu, N., and Sieck, G. C. (2021) TNFalpha induces mitochondrial fragmentation and biogenesis in human airway smooth muscle. *Am. J. Physiol. Lung Cell Mol. Physiol.* **320**, L137–L151
97. Wang, W., Wang, Y., Long, J., Wang, J., Haudek, S. B., Overbeek, P., *et al.* (2012) Mitochondrial fission triggered by hyperglycemia is mediated by ROCK1 activation in podocytes and endothelial cells. *Cell Metab.* **15**, 186–200
98. Valente, A. J., Maddalena, L. A., Robb, E. L., Moradi, F., and Stuart, J. A. (2017) A simple ImageJ macro tool for analyzing mitochondrial network morphology in mammalian cell culture. *Acta Histochem.* **119**, 315–326